

Published in final edited form as:

*Neuroimage*. 2009 February 1; 44(3): 777–789. doi:10.1016/j.neuroimage.2008.09.051.

## Joint source based morphometry identifies linked gray and white matter group differences

Lai Xu<sup>a,b</sup>, Godfrey Pearlson<sup>c,d</sup>, and Vince D. Calhoun<sup>a,b,c,d,\*</sup>

<sup>a</sup> The Mind Research Network, 1101 Yale Boulevard, Albuquerque, New Mexico 87131, USA

<sup>b</sup> Department of ECE, University of New Mexico, Albuquerque, New Mexico 87131, USA

<sup>c</sup> Olin Neuropsychiatry Research Center, Institute of Living, Hartford, Connecticut 06106, USA

<sup>d</sup> Department of Psychiatry, Yale University School of Medicine, New Haven, Connecticut 06520, USA

### Abstract

We present a multivariate approach called joint source based morphometry (jSBM), to identify linked gray and white matter regions which differ between groups. In jSBM, joint independent component analysis (jICA) is used to decompose preprocessed gray and white matter images into joint sources and statistical analysis is used to determine the significant joint sources showing group differences and their relationship to other variables of interest (e.g. age or sex). The identified joint sources are groupings of linked gray and white matter regions with common covariation among subjects. In this study, we first provide a simulation to validate the jSBM approach. To illustrate our method on real data, jSBM is then applied to structural magnetic resonance imaging (sMRI) data obtained from 120 chronic schizophrenia patients and 120 healthy controls to identify group differences. jSBM identified four joint sources as significantly associated with schizophrenia. Linked gray–white matter regions identified in each of the joint sources included: 1) temporal — corpus callosum, 2) occipital/frontal — inferior fronto-occipital fasciculus, 3) frontal/parietal/occipital/temporal — superior longitudinal fasciculus and 4) parietal/frontal — thalamus. Age effects on all four joint sources were significant, but sex effects were significant only for the third joint source. Our findings demonstrate that jSBM can exploit the natural linkage between gray and white matter by incorporating them into a unified framework. This approach is applicable to a wide variety of problems to study linked gray and white matter group differences.

### Keywords

Gray matter and white matter; Joint source based morphometry; Joint independent component analysis; Group differences

---

\*Corresponding author. The MIND Research Network, 1101 Yale Boulevard, Albuquerque, NM 87131, USA. Fax: +1 505 272 8002., E-mail address: vcalhoun@unm.edu (V.D. Calhoun).

**Publisher's Disclaimer:** This article appeared in a journal published by Elsevier. The attached copy is furnished to the author for internal non-commercial research and education use, including for instruction at the authors institution and sharing with colleagues. Other uses, including reproduction and distribution, or selling or licensing copies, or posting to personal, institutional or third party websites are prohibited.

In most cases authors are permitted to post their version of the article (e.g. in Word or Tex form) to their personal website or institutional repository. Authors requiring further information regarding Elsevier's archiving and manuscript policies are encouraged to visit: <http://www.elsevier.com/copyright>

## Introduction

Structural magnetic resonance imaging (sMRI) is a widely used approach that provides information about brain morphometry. In order to identify group differences, sMRI images are employed to extract the regional variance. Following tissue segmentation, most previous studies treat gray and white matter tissues in separate analyses. Since gray matter is composed predominantly of neurons while white matter is composed mainly of axons connected to neurons, there should be some relationship between the changes of these two brain tissues. However, few studies have assessed group differences in both gray matter and white matter. Within those few studies, gray matter and white matter were analyzed separately by voxel based morphometry (VBM) or regions of interest (ROI) to detect regions showing group differences (Wright et al., 1995; Mitelman et al., 2007a) and then correlation analysis was used to examine correlated changes between the detected gray and white matter regions (Schneider-Axmann et al., 2006). For ROI analyses, this generally requires manual drawing of the regions, although computational parcellation methods provide a way forward if white matter atlases can be incorporated (Makris et al., 2006). For VBM analysis, the region determination is based on individual voxels and no cross voxel information is used. Further, the correlation analysis can only be carried out between individual voxels or averages within prespecified ROIs. In order to efficiently find naturally clustered regions that reveal linked gray and white matter group differences throughout the whole brain, we developed a novel method termed joint source based morphometry (jSBM). In this method, the gray and white matter changes are “linked” in that they show the same intersubject covariation.

JSBM is an extension of source based morphometry (SBM) (Xu et al., 2008). Here, the “source” comprises several regions which together exhibit intersubject covariance and group difference. In SBM, three fundamental steps are required, preprocessing, independent component analysis and statistical analysis. First, the raw images are preprocessed identically to voxel based morphometry (VBM) (Good et al., 2001). Then independent component analysis (ICA) is used to the preprocessed images to derive the spatially independent sources. Finally, the sources are subjected to statistical analysis to determine the significant sources that show group differences, remove noise, and analyze the effect of other variables of interest (such as age and sex). SBM incorporates cross voxel information in sMRI images by utilizing the multivariate approach ICA. By replacing the ICA step in SBM with joint ICA, we extend SBM to jSBM, which performs gray and white matter joint analysis and aims to identify linked gray and white matter group differences. A schematic describing the jSBM approach is shown in Fig. 1.

Joint ICA is the kernel of jSBM. It is a data fusion method which can combine multiple types of data from the same participants and extract their correlated information (Calhoun et al., 2006a; Calhoun and Adali, in press). In jSBM, after preprocessing procedure, segmented gray matter and white matter images can be extracted from one sMRI image. Then it becomes possible to use joint ICA to fuse gray and white matter images from the same subject. We assume that a small number of joint sources in the brain would show linked gray and white matter differences between groups. The joint sources are maximally spatially independent and each corresponds to a set of gray matter regions and a set of white matter regions. The gray matter regions and white matter regions within one joint source share the same contribution to the intersubject covariation and hence capture the linked gray matter and white matter group differences. A statistical analysis is then used to detect the joint sources showing significant group differences.

In this paper, we first validate the jSBM concept using a simulation. Next, we describe jSBM in detail and apply it to a real sMRI data set from healthy controls and schizophrenia patients. Since schizophrenia is a well known complex mental illness which affects multiple brain regions including both gray matter and white matter (Shenton et al., 2001), it is likely that

linked gray and white matter abnormalities are manifested in this mental illness. Moreover, multiple previous studies in schizophrenia can be drawn to help us evaluate the jSBM performance. For example, Pearlson (1997) performed a selective review on the structural brain imaging in schizophrenia, and Shenton et al. (2001) contained recent MRI findings in schizophrenia, both of which reviewed a large number of regional abnormalities in schizophrenia. In addition, Davis et al. (2003) focused on white matter changes and Kubicki et al. (2007) performed a review of diffusion tensor imaging studies in schizophrenia. Based upon these papers and others, we expected corpus callosum and thalamus to be identified in the joint sources. Since these two subcortical tissues have complex interconnections with other regions, the abnormalities in these tissues would likely be related to disturbances in the circuits of multiple structural systems and hence be linked to gray matter changes in these circuits (Andreasen, 1997; Bynet et al., 2008; Walterfang et al., 2008). Also we predicted that white matter abnormalities would be detectable in some white matter tracts connecting to cerebral cortex (Kubicki et al., 2007) such as the superior longitudinal fasciculus (Seok et al., 2007; Caprihan et al., 2008) and would be linked to other white matter as well as gray matter relative changes.

## Simulation

In order to evaluate the jSBM algorithm we performed a simulation (see Fig. 2). The simulation was designed to contain a variety of changes in gray and white matter that might be interesting in identifying group difference studies. In the simulation, five different types of joint sources (a set of linked gray and white matter regions) were simulated: 1) a joint source showing more linked gray matter (GM) and white matter (WM) in group 1 than in group 2; 2) a joint source with less linked GM and WM in group 1 than in group 2; 3) a joint source with the same GM and WM between the two groups; 4) a joint source only showing GM differences between the two groups; and 5) a joint source showing only WM differences between the two groups. In some special cases, the gray/white matter regions had a strong covariation which was not shared by white/gray matter regions and the white/gray matter voxels has a value near zero for that joint source, for example, joint source 4 and 5. JSBM aims to detect all the joint sources and statistical analysis identified the joint sources showing significant group differences. The detailed design and results are as follows.

First, we generated two 256 by 256 images to simulate GM and WM separately. Then 8 circular regions were generated, each with a radius of 25 voxels and standard deviation of 6 voxels. Region 1–4 were within the GM image, region 5–8 were within the WM image. Next, we created 100 GM and 100 WM images for group 1 (see Fig. 2a) and group 2 (see Fig. 2b) separately to represent GM and WM of 100 subjects. For group 1, the intensities of regions 1–8 were uniformly distributed between 95% and 105% of the original circular region intensity. Hence these 8 regions only had slight differences from subject to subject within group 1. For group 2, the intensities of region 1 were uniformly distributed between 60% and 70% of the original circular region intensity, the intensities of region 2 were uniformly distributed between 130% and 140% of the original circular region intensity, the intensities of region 3 were uniformly distributed between 95% and 105% of the original circular region intensity, the intensities of region 4 were uniformly distributed between 80% and 90% of the original circular region intensity, the intensity distribution parameters of region 5 were the same as region 2, the intensity distribution parameters of region 6 were the same as region 3, the intensity distribution parameters of region 7 were the same as region 1, and the intensities of region 8 were uniformly distributed between 150% and 160% of the original circular region intensity.

A jSBM analysis was carried out on these 400 images in order to evaluate its performance. Fig. 2c shows the jSBM result thresholded at  $|Z| > 3.0$ . The five joint sources were all correctly estimated. Joint source 1 included region 1 of gray matter and region 7 of white matter, which

showed a 30%–40% decrease in group 2 versus group 1. Joint source 2 included region 2 of gray matter and region 5 of white matter, which linked with 30%–40% more in group 2 than in group 1. Joint source 3 included region 3 of gray matter and region 6 of white matter, which were similar among the groups. Joint source 4 only included region 4 of gray matter which was 10%–20% less in group 2 than in group 1. Joint source 5 only included region 8 with white matter showing a 50%–60% increase in group 2 versus group 1. Joint source 1–3 included both gray and white matter regions reflecting gray and white matter linked covariance. Joint source 4 and 5 consisted of only gray or white matter, respectively. For joint source 4, the gray matter region had a strong covariation which was not shared by a white matter region and the white matter voxels in the joint source appropriately had a value near zero. For joint source 5, the white matter region had a strong covariation which was not shared by a gray matter region.

We then performed a two sample *t*-test on the loading parameters obtained by jSBM in order to evaluate differences between group 1 and group 2. Joint sources 1, 2, 4, and 5 showed significant group differences with  $p < 0.05$ . Joint source 3 had a *p* value greater than 0.40, which meant although the regions in gray and white matter shared the same intensity loading parameter, they did not show significant differences between groups. Therefore, joint sources 1, 2, 4, and 5 showing significant group differences were kept as the final jSBM results.

This simple yet effective simulation demonstrates the concept behind jSBM to find joint gray matter and white matter sources that represent linked gray and white matter differences between groups, i.e., the regions in gray matter have similar intersubject covariation as the white matter regions. Next we give a more detailed description of the jSBM method. We also show an application of jSBM to identify the linked gray matter and white matter differences between schizophrenia patients and healthy controls.

## Materials

### Participants

One hundred and twenty participants with schizophrenia (SZ) (mean age = 42.1, SD = 12.9, range 20–81, 51 females) and 120 matched healthy controls (mean age = 42.7, SD = 16.6, range 18–78, 65 females) were scanned at Johns Hopkins University. Exclusion criteria for all participants included a history of overt brain disease, mental retardation, head injury with loss of consciousness for greater than 30 min, or a diagnosis of substance abuse within the last year or lifetime substance dependence. Healthy participants were recruited using random-digit dialing as part of Phase 1 of the Johns Hopkins Aging, Brain Imaging, and Cognition (ABC) study (Schretlen et al., 2000). All healthy controls were screened to ensure they were free from DSM-III-R/DSM-IV Axis I or Axis II psychopathology (SCID) (Spitzer et al., 1989; First et al., 1997). Patients met criteria for DSM-IV schizophrenia on the basis of a SCID diagnosis and review of the case file. All patients with schizophrenia were stable and taking antipsychotic medications (the exact medication information was not available for these data). These data were previously analyzed using source based morphometry (Xu et al., 2008).

### Imaging parameters

Whole brain sMRIs were obtained on a single 1.5 T scanner (Signa; GE Medical Systems, Milwaukee, WI). The whole brain was evaluated in the coronal plane using a spoiled GRASS 3D imaging sequence, with the following imaging parameters: 35 ms TR, 5 ms TE, 45° flip angle, 1 excitation, 1.5 mm slice thickness, 24 cm field of view, and a matrix size of 256×256.

## Methods

### Image preprocessing

The images were preprocessed by the preprocessing steps used for VBM approach (Ashburner and Friston 2000, 2001, 2005) and employed the Matlab program SPM5 (Statistical Parametric Mapping, Wellcome Institute, London, UK). Images were normalized to the 152 average T<sub>1</sub> Montreal Neurological Institute (MNI) template, interpolated to voxel dimensions of 1.5×1.5×1.5 mm and segmented into gray matter, white matter and cerebrospinal fluid (CSF) compartments. Registration, bias correction and tissue classification are combined within one generative model which is based on image intensity, nonuniformity and tissue probability maps. The model parameter estimation aims to maximize the posteriori solution and involves alternating among classification, bias correction and registration steps (Ashburner and Friston 2005). The gray matter and white matter images were then smoothed separately with 12 mm full width at half-maximum (FWHM) Gaussian kernel. Each voxel in a smoothed image contains the averaged partial volume of gray matter or white matter from around and within the selected voxel, which contains gray or white matter concentration, a value ranging from 0 to 1. The original dimension of the gray/white matter images is 121×145×121. These images were then analyzed with jICA.

### Joint independent component analysis

Every gray matter image was converted to a one-dimensional vector. The 120 gray matter image vectors of healthy controls and 120 gray matter image vectors of schizophrenia patients were then arrayed into one 240 row subject–graymatter matrix  $G$ . The same was done to the 240 white matter images to get the subject–whitematter matrix  $W$ . The dimensionality of  $G$  and  $W$  were both 240 by 425,389. Note that 425,389 is smaller than the original dimensionality of 121×145×121=2,122,945 since non-brain voxels were excluded. These two matrices were next stacked horizontally into a subject–voxel matrix  $X=[G\ W]$  (see Fig. 3). The dimensionality of  $X$  is then 240 by 850778. A modified Akaike's information criterion (AIC) (Akaike 1974; Li et al., 2007) was used to estimate the number of joint sources,  $k$ , from matrix  $X$  (Calhoun et al., 2001). The subject–voxel matrix  $X$  was then decomposed linearly into a subject–source mixing matrix  $A$  and a source–voxel source matrix  $S$  using spatial ICA (Calhoun et al., 2001). ICA was performed using the infomax algorithm, which attempts to minimize the mutual information of the output sources (Bell and Sejnowski 1995; Lee et al., 1999). The source matrix  $S$  was then separated horizontally into a source–graymatter matrix  $S_G$  and a source–whitematter matrix  $S_W$ , i.e.,  $X=[G\ W]=A\cdot S=A\cdot[S_G\ S_W]$ . Every row of the source matrix corresponds to a joint source including both gray matter regions and white matter regions. The source matrix expresses the relationship between the  $k$  joint sources and the voxels within the brain. The gray matter regions and white matter regions within one joint source have the same shared contribution to the subjects captured by loading parameters within the mixing matrix. Therefore, the joint source indicates the joint gray matter regions and white matter regions which are related by the same intersubject covariation. The mixing matrix expresses the relationship between subjects and  $k$  joint sources. The rows of the mixing matrix are scores that indicate the relative degree each of the  $k$  joint sources contributes to a given subject. The columns of the mixing matrix indicate how one joint source contributes to each of the 240 subjects.

### Statistical analysis

We performed a statistical analysis to the mixing matrix. Since every column of the mixing matrix contains the loading parameters expressing the contribution of every joint source to the 240 subjects, a two sample  $t$ -test can be used to every column of the mixing matrix to test which joint source shows a difference between healthy control and schizophrenia. A corrected

threshold of  $p < 0.05$  which controls for the false discovery rate (FDR) was used to determine the most significant joint sources (Genovese et al., 2002).

The effects of age and sex on the significant sources were also determined. We regressed the columns of the mixing matrix on age and sex using a threshold of  $p < 0.05$  to determine the joint sources that were significantly correlated with age or sex. In order to verify that the group differences in the significant sources were still present after removing the effect of age and sex, we computed a two sample  $t$ -test on the residual of the regression and tested the difference between controls and patients.

## Visualization

We used the source matrix for visualization. Each row of the source matrix was scaled to unit standard deviation. Then its left half (gray matter regions) and right half (white matter regions) were reshaped into two 3D images separately. Thus, for one row of the source matrix we have one gray matter region map and one white matter region map, the two maps together form a joint source map. The significant joint source maps were then superimposed on the MNI normalized template brain and thresholded at  $|Z| > 3.0$ . The regions within the most significant joint sources were labeled by transforming from the MNI coordinate system to the coordinates of the standard space of Talairach and Tournoux (1988) using a Matlab conversion program written by Matthew Brett (<http://imaging.mrc-cbu.cam.ac.uk/downloads/MNI2tal>, MRC Cognition and Brain Sciences Unit, Cambridge, England). Once converted, the Talairach coordinates were entered into the Talairach Daemon (Lancaster et al., 2000) and summarized. In addition, the white matter regions within significant joint sources were thresholded at  $|Z| > 3.0$  and specifically labeled using the ICBM DTI-81 Atlas (Mori et al., 2008).

## Results

The number of sources was estimated to be forty using the modified AIC approach. The mixing matrix and source matrix were decomposed using joint ICA. The mixing matrix was then analyzed using the two sample  $t$ -test for patients versus controls. Seven joint sources whose loading parameters in mixing matrix differed significantly between controls and patients were identified. On visual inspection of the seven joint source maps, three sources appeared to be obvious artifacts showing sharp edges near the brain boundary or appearing within CSF regions. Within the remained four joint sources, the loading parameters in mixing matrix of joint source 1 and joint source 2 are lower in patients, whereas the loading parameters of joint source 3 and joint source 4 are higher in patients. Figs. 4 and 5 show the joint sources. Joint source 1 and joint source 2 are displayed in Fig. 4, using blue for joint source 1, green for joint source 2 and cyan for the overlap. Joint source 3 and joint source 4 are displayed in Fig. 5, using red for joint source 3, yellow for joint source 4 and orange for the overlap. The identified joint sources each include regions which reflect group differences in their covariation among subjects. The Talairach coordinates for the four significant joint sources are listed in Table 1. The white matter determined by ICBM DTI-81 Atlas is listed in Table 2. The age and sex effects on these four joint sources were also analyzed.

### Anatomy of the significant joint sources

For convenience, the four significant joint sources are listed by a summary of their anatomical regions and represented in order of increasing  $p$  values (decreasing significance). Only the regions with positive contribution to the covariance were represented within the joint sources to prevent duplicate information from the regions with negative contribution (opposite covariance). Note that since each joint source represents a set of regions which have common intersubject covariation, the short anatomic label does not fully describe the source.

### Joint source 1: temporal — corpus callosum

The largest difference in gray and white matter linked changes between healthy controls and patients was found within joint source 1 (see Fig. 4, blue and cyan blob) with less gray matter and white matter in schizophrenia patients. The regions include the bilateral superior temporal gyrus, insula, anterior cingulate, cingulate gyrus, inferior and medial frontal gyri in gray matter, and white matter in splenium of corpus callosum, close proximity to posterior cingulate, hippocampus, parahippocampal gyrus, medial and middle frontal gyri. According to the Talairach table, the abnormal gray matter volume is 207.6 cc, the abnormal white matter volume is 16.3 cc.

### Joint source 2: occipital/frontal — IFO

Joint source 2 (see Fig. 4, green and cyan blob) shows a second significant difference between healthy controls and patients with schizophrenia having more gray matter in middle and inferior occipital gyri, insula, middle and inferior frontal gyri, middle and inferior temporal gyri and cuneus, and white matter in inferior fronto-occipital fasciculus (IFO), precuneus and close proximity to middle frontal gyrus. According to the Talairach table, the abnormal gray matter volume is 19.8 cc, the abnormal white matter volume is 22.4 cc.

### Joint source 3: frontal/parietal/occipital/temporal — SLF

Joint source 3 (see Fig. 5, red and orange blob) was found to have more linked gray matter and white matter changes in patients versus healthy controls. It includes supramarginal gyrus, inferior parietal lobule, middle temporal gyrus, media and middle frontal gyri and parahippocampal gyrus in gray matter, and white matter in superior longitudinal fasciculus (SLF), close proximity to superior and middle temporal gyri, supramarginal gyrus and inferior parietal lobe. According to the Talairach table, the abnormal gray matter volume is 50.4 cc, the abnormal white matter volume is 133.3 cc.

### Joint source 4: parietal/frontal — thalamus

Within joint source 4 (see Fig. 5, yellow and orange blob), the patients show more gray matter in inferior parietal lobule, postcentral gyrus, middle media and superior frontal gyri, and more white matter in thalamus and cuneus than healthy controls. According to the Talairach table, the abnormal gray matter volume is 47.2 cc, the abnormal white matter volume is 110.9 cc.

### Age and sex effect

The effects of age on all the four joint sources are significant at  $p < 0.001$ . The correlation plots of age versus ICA weights for the four joint sources are presented in Fig. 6. For joint source 1, the ICA weight decreases as age increases. According to the linear trend, the intercept value of the controls is slightly higher than that of patients and the negative slope value of the controls is slightly lower than that of the patients. For joint source 2, the ICA weight decreases as age increases. The intercept values of controls and patients are nearly the same, the negative slope value of controls is nearly zero and slightly higher than that of patient. For joint source 3, the ICA weight increases as age increases. According to the linear trend, the intercept values of controls and patients are nearly the same, the positive slope value of controls is nearly zero and slightly lower than that of patient. For joint source 4, the ICA weight decreases as age increases. According to the linear trend, the intercept values of controls and patients are nearly the same, the negative slope value of patients is nearly zero and slightly higher than that of patient.

The effect of sex was significant only on joint source 3 at  $p < 0.00005$  as presented in Fig. 7. The mean of the ICA weight for the males is larger than that for the females of both healthy controls and patients. The overall mean of patients is 0.0066 which is slightly larger than that

of the healthy controls 0.0062. The relationship of the means for males (M), females (F), healthy controls (HC) and patients (SZ) is  $M_{SZ} (0.0068) > M_{HC} (0.0066) > F_{SZ} (0.0064) > F_{HC} (0.0059)$ .

After removing the effect of age and sex, the group differences in the joint sources remained significant.

## Discussion

We present a jSBM approach to identify joint sources that differ significantly between groups. The gray and white matter regions within one joint source have the same contribution to intersubject covariation, which reflects linked gray and white matter changes among individuals.

For joint source 1, the finding of less gray matter in temporal and frontal gyri and their intercorrelations are consistent with previous findings (Pearlson, 1997; Gur et al., 2000; Mitelman et al., 2005). The smaller corpus callosum in white matter agrees with previous reports (Bachmann et al., 2003; Diwadkar et al., 2004). The smaller hippocampus is also consistent with previous findings (Velakoulis et al., 2006; Vita and de Peri, 2007). The linkage between less gray matter in temporal lobe and the lesser white matter in corpus callosum is interesting and may be related to the posterior corpus callosum connections to temporal lobe (Woodruff et al., 1993; Downhill et al., 2001; Walterfang et al., 2008).

For joint source 2, the gray matter reduction in middle occipital gyrus and cuneus agrees with reports by others (Andreasen et al., 1994; Narr et al., 2005). The white matter reduction in inferior fronto-occipital fasciculus is supported by previous reports (Mitelman et al., 2007b; Cheung et al., 2008). Our findings suggest the precuneus, which has not been well studied, might also be a key area in the regional brain abnormalities which underlie the disease. We also suggest the gray matter reduction in prefrontal cortex and occipital gyrus may be linked to the dysfunction of inferior fronto-occipital fasciculus.

For joint source 3, more gray and white matter have been detected affecting multiple brain lobes, reflecting the widespread nature of the disease and consistent with previous findings (Shenton et al., 2001). The abnormality of superior longitudinal fasciculus is consistent with previous studies (Seok et al., 2007; Caprihan et al., 2008; Karlsgodt et al., 2008). Since the superior longitudinal fasciculus connects the frontal, occipital, parietal and temporal lobes, its abnormality might be an important contributor to gray matter abnormalities in these brain regions (Shergill et al., 2007).

For joint source 4, the larger thalamic white matter concentrations in schizophrenia might be related to abnormalities of the synapses connected to the thalamic nuclei. Although most of the studies have been focused on the gray matter in thalamus (Byne et al., 2008), our study suggests the thalamic white matter might also play an important role in receiving and projecting information between the thalamus and particular cortical fields. Future studies incorporating diffusion tensor imaging might help test this hypothesis. The larger gray matter in parietal and frontal lobes associated with altered white matter is consistent with earlier work, but may be related to complex shape changes and require computational anatomy to clarify (Calhoun et al., 2006b). Our findings also suggest gray matter difference in the parietal and frontal lobe are linked to white matter difference in thalamus which is consistent with the role of the thalamus as a relay station.

The overall gray matter and white matter volumes within each joint source were calculated from the Talairach tables. It is interesting to note that most of the control>patient regions are in gray matter, whereas most of the patient>control regions are in white matter in every joint

source except joint source 2. The lesser gray matter and more white matter in schizophrenia is consistent with previous reports (Mitelman et al., 2007a). This finding might be due to the disruption of white matter integrity (leading to more white matter) in patients which in turn results in a reduction of gray matter. We hope to investigate the underlying cause in future work.

Every joint source reveals a set of linked gray and white matter regions that have a significant difference between schizophrenia and healthy controls. The independent joint sources reflect the group difference of various combinations of brain regions. Though the four joint sources are spatially independent, this does not mean that they are necessarily non-overlapping. Indeed, we found some interesting overlaps between joint source 1 and joint source 2 and also between joint source 3 and joint source 4 when examining the Talairach tables and figures (cyan blob in Fig. 4 and orange blob in Fig. 5). It should be noted that the fact that they appear in different joint sources means that their intersubject covariation is distinct. The overlapping regions appearing in different sources may underlie aspects of higher cortical function such as language and executive function that appear to be most disturbed in schizophrenia patients. Since it is not likely that all brain regions contribute to only a single joint source, these overlapping regions may well be involved in multiple sources corresponding to different functional connectivities. For example, the middle and medial frontal gyri showed disturbance in all four joint sources, indicating their multifunctional/integrative roles. The insula was observed in all the four joint sources, implying its role in various highly conserved functions. In addition, the inferior parietal lobe found in joint sources 3 and 4, the posterior cingulate cortex found in joint sources 1 and 2, precuneus found in all joint sources, are frequently found to be structurally or functionally altered in individuals with schizophrenia.

All four joint sources were significantly correlated with age. Though this study is cross-sectional and not longitudinal, we can still look more closely at the age-related changes. For joint source 1, the intercept and slope suggest the source concentration in patients is smaller than in controls at early ages; however it declines slower than controls with increasing age. By age 75, the source concentration reaches a similar size for both patients and controls. For joint sources 2, 3 and 4, the source concentration in patients and controls are similar at early ages. However, for joint source 2, the source concentration in patient declines faster than controls with increasing age. At older ages, the source concentration in the patients becomes smaller than in controls. For joint source 3, the source concentration in patient increases at early ages and continues declining with increasing age. At older ages, the source concentration in patients becomes larger than in controls. For joint source 4, the source concentration in controls begins to decrease at early ages while the source concentration in patients is nearly stable. At older ages, the source concentration in controls becomes smaller than in patients. A significant sex effect was found for joint source 3. The mean difference between male and female for both healthy controls and patients implies the source concentration of males is greater than that of females.

There are also some limitations of the jSBM approach which should be mentioned. First, the assumption of the same linear covariation for gray and white matter is fairly strong, although it appears to provide meaningful results in the simulation and schizophrenia application. Because it is possible that the joint sources may also show more complicated and/or nonlinear relationships, we would like to relax this linear assumption in our future work. It should also be noted that the preprocessing steps will likely have an impact on the results. Though we have applied the typical preprocessing used in VBM for this work, future work should investigate the impact of different preprocessing steps. We did compare different smoothing amounts between 8 mm and 12 mm and found the results to be largely consistent (not shown), however additional preprocessing and segmentation choices should be investigated. Finally, our

approach only considered the gray and white matter segmented images. It would be interesting to include an additional compartment for CSF, which we plan to pursue in future work.

## Conclusion

In summary, jSBM provides a unified framework which exploits the natural linkage between gray and white matter to identify joint gray and white matter sources that show group differences. Our initial experience with jSBM provided some new and interesting insights which merit further study. JSBM is a multivariate approach for image fusion among different types of structural MRI images which is applicable to a wide array of questions, including gray and white matter joint analysis, the identification of group differences, or the association of joint gray and white matter differences with other variables of interest (e.g. age or sex). In addition, jSBM can also filter out spatial artifactual sources and separate them from the sources of interest. For the above reasons, jSBM may provide a powerful new tool for analysis of structural brain images.

## Acknowledgments

We would like to thank Arvind Caprihan for his helpful comments and suggestions. This study was funded by the National Institutes of Health grants: 1 R01 EB 000840 and 1 R01 EB 005846 (to VC), NSF-IIS Award no: 0612076 (to VC), and 2 R01 MH43775 MERIT Award, 5 R01 MH52886 and a NARSAD Distinguished Investigator Award (to GP).

## References

- Akaike H. A new look at statistical model identification. *IEEE Trans Automat Contr* 1974;19:716–723.
- Andreasen NC. The role of the thalamus in schizophrenia. *Can J Psychiatry* 1997;42(1):27–33. [PubMed: 9040920]
- Andreasen NC, Flashman L, et al. Regional brain abnormalities in schizophrenia measured with magnetic resonance imaging. *JAMA* 1994;272(22):1763–1769. [PubMed: 7966925]
- Ashburner J, Friston KJ. Voxel-based morphometry—the methods. *NeuroImage* 2000;11(6 Pt 1):805–821. [PubMed: 10860804]
- Ashburner J, Friston KJ. Why voxel-based morphometry should be used. *NeuroImage* 2001;14(6):1238–1243. [PubMed: 11707080]
- Ashburner J, Friston KJ. Unified segmentation. *NeuroImage* 2005;26(3):839–851. [PubMed: 15955494]
- Bachmann S, Pantel J, et al. Corpus callosum in first-episode patients with schizophrenia—a magnetic resonance imaging study. *Psychol Med* 2003;33(6):1019–1027. [PubMed: 12946086]
- Bell AJ, Sejnowski TJ. An information–maximization approach to blind separation and blind deconvolution. *Neural Comput* 1995;7(6):1129–1159. [PubMed: 7584893]
- Byne W, Hazlett EA, et al. The thalamus and schizophrenia: current status of research. *Acta Neuropathol*. 2008(Electronic publication ahead of print)
- Calhoun VD, Adali T. Feature-based Fusion of Medical Imaging Data. *IEEE Trans Inf Tech in Biomedicine*. in press
- Calhoun VD, Adali T, et al. A method for making group inferences from functional MRI data using independent component analysis. *Hum Brain Mapp* 2001;14(3):140–151. [PubMed: 11559959]
- Calhoun VD, Adali T, et al. A method for multitask fMRI data fusion applied to schizophrenia. *Hum Brain Mapp* 2006a;27(7):598–610. [PubMed: 16342150]
- Calhoun VD, Adali T, et al. Method for multimodal analysis of independent source differences in schizophrenia: combining gray matter structural and auditory oddball functional data. *Hum Brain Mapp* 2006b;27(1):47–62. [PubMed: 16108017]
- Caprihan A, Pearlson GD, et al. Application of principal component analysis to distinguish patients with schizophrenia from healthy controls based on fractional anisotropy measurements. *NeuroImage* 2008;42(7):675–682. [PubMed: 18571937]

- Cheung V, Cheung C, et al. A diffusion tensor imaging study of structural dysconnectivity in never-medicated, first-episode schizophrenia. *Psychol Med* 2008;38(6):877–885. [PubMed: 17949516]
- Davis KL, Stewart DG, et al. White matter changes in schizophrenia: evidence for myelin-related dysfunction. *Arch Gen Psychiatry* 2003;60(5):443–456. [PubMed: 12742865]
- Diwadkar VA, DeBellis MD, et al. Abnormalities in MRI-measured signal intensity in the corpus callosum in schizophrenia. *Schizophr Res* 2004;67(2–3):277–282. [PubMed: 14984888]
- Downhill JE Jr, Buchsbaum MS, et al. Temporal lobe volume determined by magnetic resonance imaging in schizotypal personality disorder and schizophrenia. *Schizophr Res* 2001;48(2–3):187–199. [PubMed: 11295372]
- First, MB.; Spitzer, RL., et al. Structured Clinical Interview for DSM-IV Axis I Disorders —Clinical Version (SCID-IV). American Psychiatric Press; Washington, D.C.: 1997.
- Genovese RC, Lazar AN, et al. Thresholding of statistical maps in functional neuroimaging using the false discovery rate. *NeuroImage* 2002;15:870–878. [PubMed: 11906227]
- Good CD, Johnsrude IS, et al. A voxel-based morphometric study of ageing in 465 normal adult human brains. *NeuroImage* 2001;14(1 Pt 1):21–36. [PubMed: 11525331]
- Gur RE, Cowell PE, et al. Reduced dorsal and orbital prefrontal gray matter volumes in schizophrenia. [erratum appears in *Arch Gen Psychiatry* 2000 Sep;57 (9):858]. *Arch Gen Psychiatry* 2000;57(8):761–768. [PubMed: 10920464]
- Karlsgodt KH, van Erp TG, et al. Diffusion tensor imaging of the superior longitudinal fasciculus and working memory in recent-onset schizophrenia. *Biol Psychiatry* 2008;63(5):512–518. [PubMed: 17720147]
- Kubicki M, McCarley R, et al. A review of diffusion tensor imaging studies in schizophrenia. *J Psychiatr Res* 2007;41(1–2):15–30. [PubMed: 16023676]
- Lancaster JL, Woldorff MG, et al. Automated Talairach atlas labels for functional brain mapping. *Hum Brain Mapp* 2000;10(3):120–131. [PubMed: 10912591]
- Lee TW, Girolami M, et al. Independent component analysis using an extended infomax algorithm for mixed subgaussian and supergaussian sources. *Neural Comput* 1999;11:417–441. [PubMed: 9950738]
- Li YO, Adali T, et al. Estimating the number of independent components for functional magnetic resonance imaging data. *Hum Brain Mapp* 2007;28(11):1251–1266. [PubMed: 17274023]
- Makris N, Kaiser J, et al. Human cerebral cortex: a system for the integration of volume- and surface-based representations. *NeuroImage* 2006;33(1):139–153. [PubMed: 16920366]
- Mitelman SA, Shihabuddin L, et al. Cortical intercorrelations of temporal area volumes in schizophrenia. *Schizophr Res* 2005;76(2–3):207–229. [PubMed: 15949654]
- Mitelman SA, Brickman AM, et al. A comprehensive assessment of gray and white matter volumes and their relationship to outcome and severity in schizophrenia. *NeuroImage* 2007a;37(2):449–462. [PubMed: 17587598]
- Mitelman SA, Torosjan Y, et al. Internal capsule, corpus callosum and long associative fibers in good and poor outcome schizophrenia: a diffusion tensor imaging survey. *Schizophr Res* 2007b;92(1–3):211–224. [PubMed: 17329081]
- Mori S, Oishi K, et al. Stereotaxic white matter atlas based on diffusion tensor imaging in an ICBM template. *NeuroImage* 2008;40(2):570–582. [PubMed: 18255316]
- Narr KL, Toga AW, et al. Cortical thinning in cingulate and occipital cortices in first episode schizophrenia. *Biol Psychiatry* 2005;58(1):32–40. [PubMed: 15992520]
- Pearlson GD. Superior temporal gyrus and planum temporale in schizophrenia: a selective review. *Prog Neuro-Psychopharmacol Biol Psychiatry* 1997;21(8):1203–1229.
- Schneider-Axmann T, Kamer T, et al. Relation between cerebrospinal fluid, gray matter and white matter changes in families with schizophrenia. *J Psychiatr Res* 2006;40(7):646–655. [PubMed: 16019030]
- Schretlen D, Pearlson GD, et al. Elucidating the contributions of processing speed, executive ability, and frontal lobe volume to normal age-related differences in fluid intelligence. *J Int Neuropsychol Soc* 2000;6(1):52–61. [PubMed: 10761367]

- Seok JH, Park HJ, et al. White matter abnormalities associated with auditory hallucinations in schizophrenia: a combined study of voxel-based analyses of diffusion tensor imaging and structural magnetic resonance imaging. *Psychiatry Res* 2007;156(2):93–104. [PubMed: 17884391]
- Shenton ME, Dickey CC, et al. A review of MRI findings in schizophrenia. *Schizophr Res* 2001;49(1–2):1–52. [PubMed: 11343862]
- Shergill SS, Kanaan RA, et al. A diffusion tensor imaging study of fasciculi in schizophrenia. *Am J Psychiatry* 2007;164(3):467–473. [PubMed: 17329472]
- Spitzer, RL.; Williams, JBW., et al. Structured Clinical Interview for DSM-III-R-Patient Version (SCID-P, 5/1/89). Biometrics Research Department, New York State Psychiatric Institute; New York, NY: 1989.
- Talairach, J.; Tournoux, P. Co-Planar Stereotactic Atlas of the Human Brain: 3-Dimensional Proportional System — An Approach to Cerebral Imaging. Thieme Medical Publishers; New York, NY: 1988.
- Velakoulis D, Wood SJ, et al. Hippocampal and amygdala volumes according to psychosis stage and diagnosis: a magnetic resonance imaging study of chronic schizophrenia, first-episode psychosis, and ultra-high-risk individuals. *Arch Gen Psychiatry* 2006;63(2):139–149. [PubMed: 16461856]
- Vita A, de Peri L. Hippocampal and amygdala volume reductions in first-episode schizophrenia. *Br J Psychiatry* 2007;190:271. [PubMed: 17329755]
- Walterfang M, Wood AG, et al. Morphology of the corpus callosum at different stages of schizophrenia: cross-sectional study in first-episode and chronic illness. *Br J Psychiatry* 2008;192(6):429–434. [PubMed: 18515892]
- Woodruff PW, Pearson GD, et al. A computerized magnetic resonance imaging study of corpus callosum morphology in schizophrenia. *Psychol Med* 1993;23(1):45–56. [PubMed: 8475214]
- Wright IC, McGuire PK, et al. A voxel-based method for the statistical analysis of gray and white matter density applied to schizophrenia. *NeuroImage* 1995;2(4):244–252. [PubMed: 9343609]
- Xu L, Groth KM, et al. Source-based morphometry: The use of independent component analysis to identify gray matter differences with application to schizophrenia. *Hum Brain Mapp*. 2008Electronic publication ahead of print

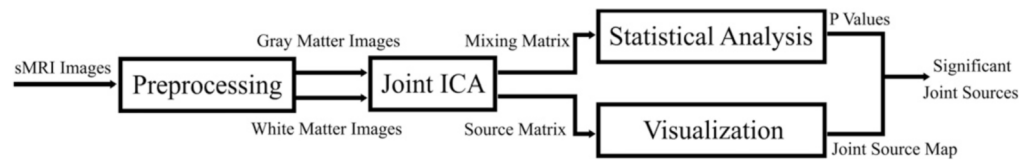


**Fig. 1.** Joint Source Based Morphometry. Structural MRI images are firstly preprocessed. Joint ICA is then applied to the segmented gray and white matter images which results in a mixing matrix and a source matrix. Statistical analysis is performed on the mixing matrix to compute the  $p$  values indicating the significance of the group differences. Visualization is carried on the source matrix to identify which regions are involved in the joint sources.

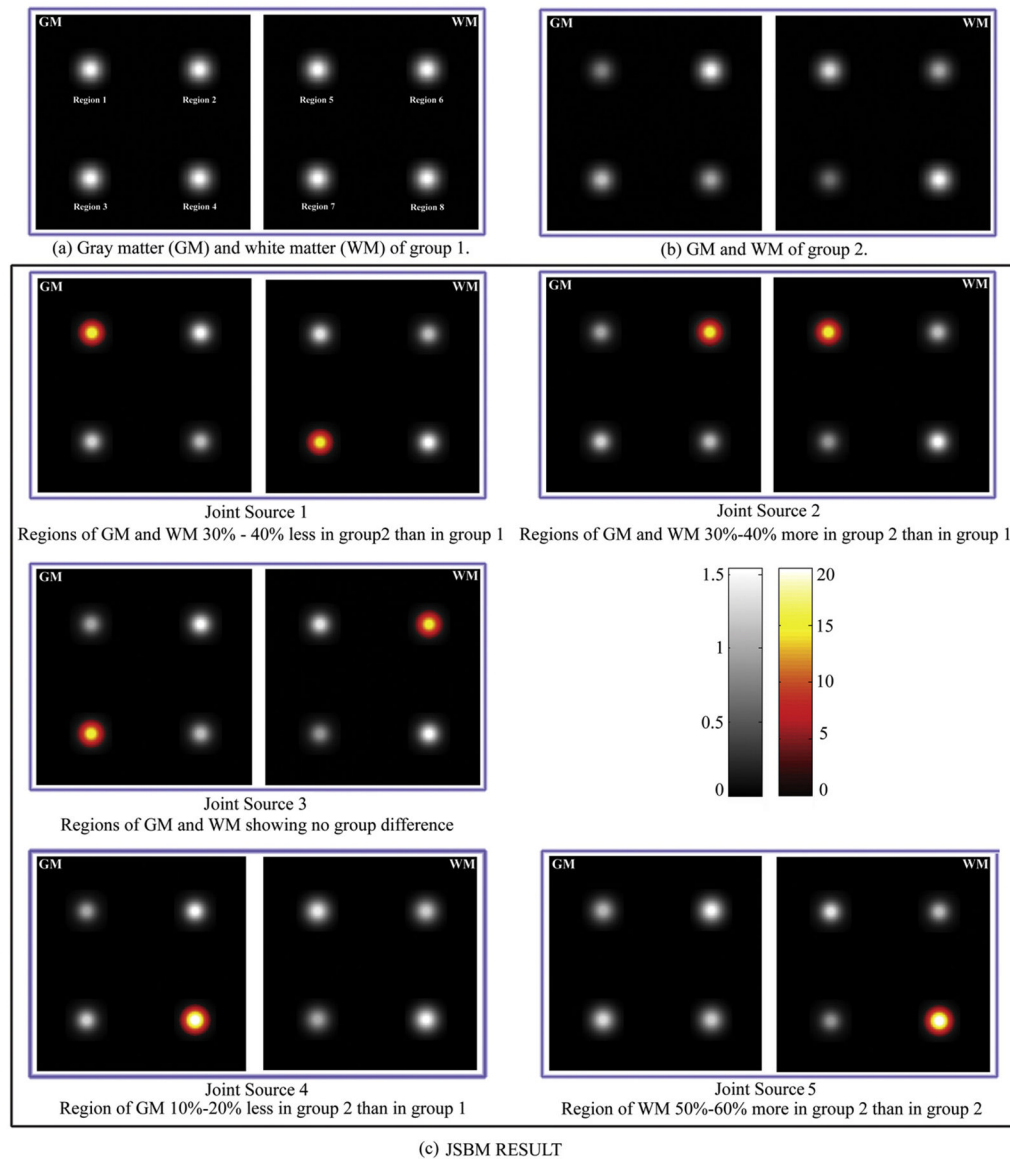


**Fig. 2.** Simulation for Joint Source Based Morphometry. (a) Simulated gray and white matter images of group 1. (b) Simulated gray and white matter images of group 2. Five different types of joint sources (a set of linked gray and white matter regions) were simulated: 1) a joint source showing more linked gray matter (GM) and white matter (WM) in group 1 than in group 2 (region 1 and region 7); 2) a joint source with less linked GM and WM in group 1 than in group 2 (region 2 and region 5); 3) a joint source with the same GM and WM between the two groups (region 3 and region 6); 4) a joint source only showing GM differences between the two groups (region 4); and 5) a joint source only showing WM differences between the two groups (region 8). Joint sources 4) and 5) were special cases, the gray/white matter regions had a strong covariation which was not shared by a white/gray matter regions. (c) JSBM result. JSBM was able to successfully detect the five different types of regions.

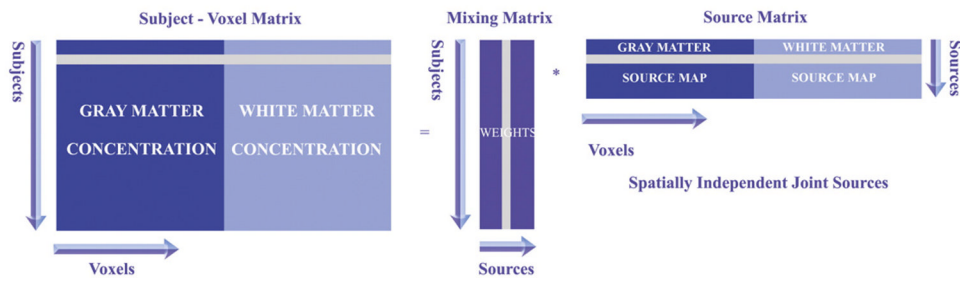


**Fig. 3.** Joint Independent Component Analysis. Gray and white matter images are stacked into one subject–voxel matrix. JICA is then used to decompose this subject–voxel matrix into a mixing matrix and a source matrix. The mixing matrix is used for statistical analysis and the source matrix is used for joint sources visualization in the following jSBM steps.

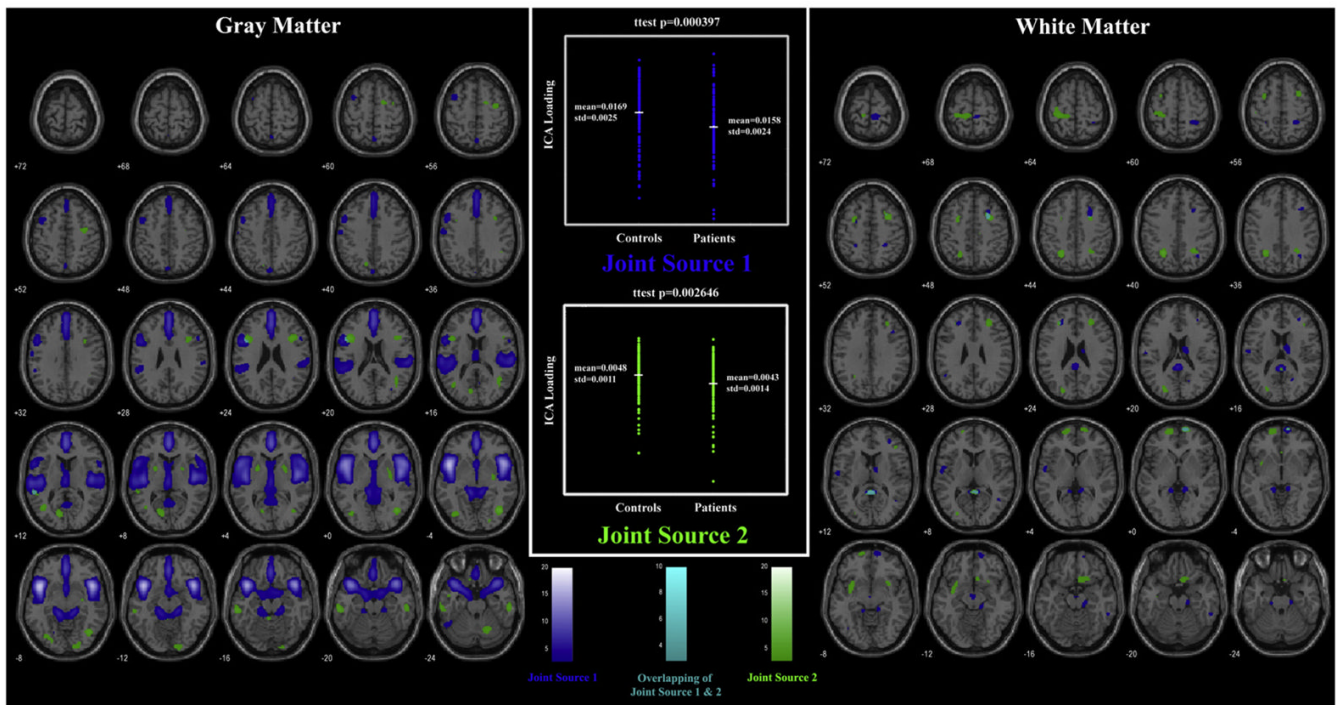


**Fig. 4.** Joint source 1 and joint source 2 discovered by jSBM thresholded at  $|Z| > 3.0$ . Left: gray matter difference; Middle: loading parameters of the joint sources; Right: white matter difference. Blue blob: Regions within joint source 1; Green Blob: Regions within joint source 2; Cyan blob: Regions within both joint source 1 and joint source 2.

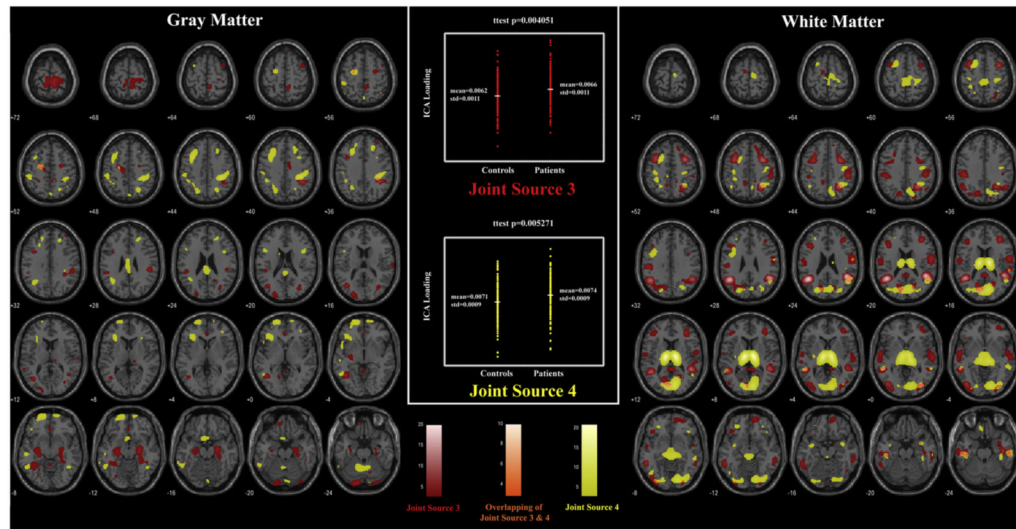


**Fig. 5.** Joint source 3 and joint source 4 discovered by jSBM thresholded at  $|Z| > 3.0$ . Left: gray matter difference; Middle: loading parameters of the joint sources. Right: white matter difference. Red blob: Regions within joint source 3; Yellow Blob: Regions within joint source 4; Orange blob: Regions within both joint source 3 and joint source 4.

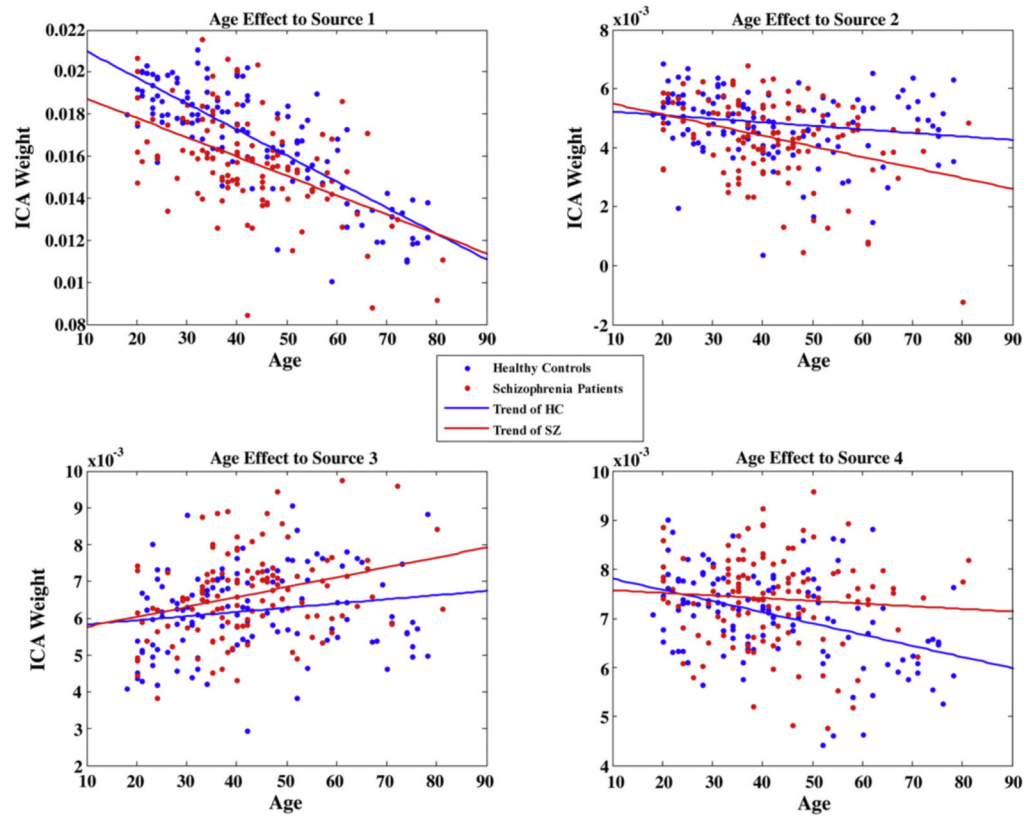


**Fig. 6.** The correlation plots between age and ICA weights for the four joint sources. Red dots: Correlation for the patients; Blue dots: Correlation for the controls; Red line: Trend for red dots; Blue line: Trend for blue dots.

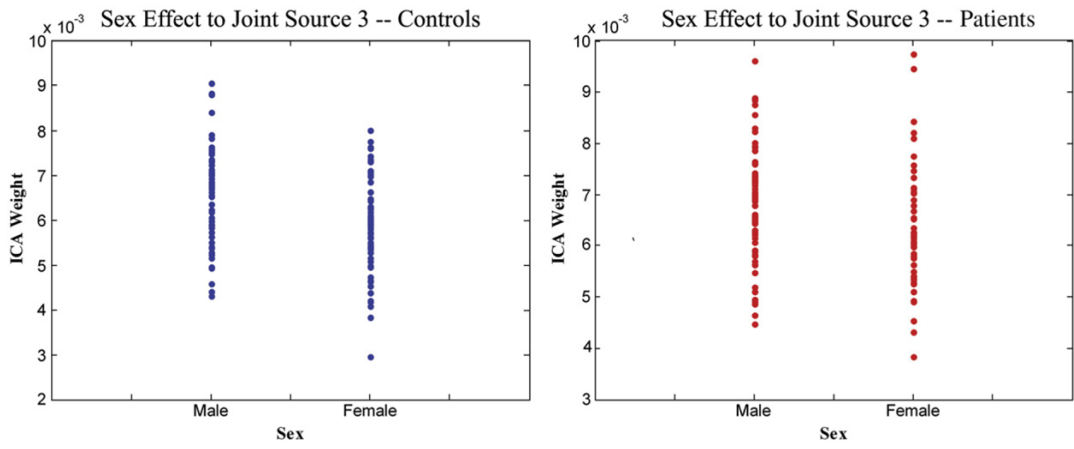


**Fig. 7.** The correlation plots between sex and ICA weights for joint source 3. Red dots: Correlation for the patients; Blue dots: Correlation for the controls.

**Table 1**  
Talairach labels for regions of the four significant joint sources

Joint source 1, gray matter	Brodmann area	L/R volume (cc)	L/R max Z(x, y, z)
Superior temporal gyrus	38, 22, 42, 41, 13, 21, 39	22.0/23.8	15.8(-46,13, -7)/17.5(45,11, -7)
Inferior frontal gyrus	47, 13, 45, 44, 9	12.3/17.9	15.1(-43,15, -11)/16.4(42,14, -11)
Insula	13, 22	8.4/10.8	11.9(-45,12, -2)/13.7(42,9, -3)
Anterior cingulate and cingulate gyrus	32, 10, 24, 25	12.1/4.4	10.2(-1,47,2)/8.7(1,42,5)
Precentral gyrus	6, 44, 43	2.2/4.1	9.9(-46, -11,7)/9.0(53,10,4)
Medial frontal gyrus	10, 9, 11, 6, 25, 8	19.0/6.9	9.6(0,53,2)/7.1(3,59,5)
Transverse temporal gyrus	42, 41	1.9/2.4	7.3(-49, -16,10)/8.2(59, -20,12)
Superior and middle frontal gyri	9, 10, 8, 11, 6, 46	3.5/5.4	7.7(0,55,25)/5.7(3,59,22)
Parahippocampal gyrus and uncus	27, 30, 34, 28, 35, 36, Amygdala, 38, 20	7.1/8.2	6.7(-12, -34, -3)/7.6(22,5, -23)
Rectal gyrus and orbital gyrus	11	1.5/0.8	7.1(0,32, -21)/5.6(4,37, -20)
Postcentral gyrus and inferior parietal lobule	40, 43, 2	4.1/3.5	7.0(-59, -21,16)/6.5(53, -26,14)
Middle and inferior temporal gyri	21, 20	1.8/0.2	6.9(-49,1, -10)/3.0(45, -20, -25)
Thalamus		5.8/3.9	6.9(0, -19,8)/5.9(1, -24,7)
Clastrum		0.6/1.9	5.4(-39, -13,2)/6.9(37,6,0)
Subcallosal gyrus	34, 25	1.9/0.6	6.0(-12,1, -15)/4.3(9,2, -15)
Caudate		1.3/1.7	4.1(-3,12,2)/4.7(3,12,2)
Posterior cingulate	30, 29, 23	2.2/1.1	4.5(-3, -52,7)/4.5(3, -46,5)
Precuneus	7, 31	0.9/0.6	3.8(-1, -61,57)/3.9(1, -77,43)
Superior occipital gyrus, cuneus and lingual gyrus	19, 30	0.4/0.4	3.5(-31, -69,21)/3.4(1, -81,39)
Joint source 1, white matter	Brodmann area	L/R volume (cc)	L/R max Z(x, y, z)
Posterior cingulate	29, 23, 30, 31	1.9/1.1	6.5(0, -40,19)/4.9(4, -43,16)
Medial and middle frontal gyri	10, 9, 6, 8, 46	3.5/0.6	4.7(-12,62, -6)/4.0(24,36,22)
Parahippocampal gyrus	30, 35, 28	1.7/0.6	4.4(-12, -38,2)/4.5(12, -39,1)
Paracentral lobule	6, 31	0.9/na	4.2(-7, -29,66)/na
Superior frontal gyrus	11, 10	0.9/0.2	4.1(-12,61, -11)/3.1(22,42,20)
Thalamus		1.1/0.2	4.1(-13, -9,17)/3.0(6, -2,10)
Angular gyrus and inferior parietal lobule	39, 40	0.6/na	4.0(-34, -58,37)/na
Caudate		0.6/na	3.6(-15, -15,19)/na
Precentral and postcentral gyri	43, 44, 5	0.8/0.8	3.5(-12, -31,69)/3.6(56, -11,13)
Middle and superior temporal gyri	39, 20, 22	0.4/0.4	3.5(-45, -55,11)/3.4(48, -52,29)
Joint source 2, gray matter	Brodmann area	L/R volume (cc)	L/R max Z(x, y, z)
Middle and inferior occipital gyri	37, 19, 18, 17	2.6/0.8	6.7(-40, -67,0)/4.6(37, -73,1)
Insula	13	0.2/1.3	3.3(-37,11,22)/5.8(40,17,18)

Joint source 1, gray matter	Brodmann area	L/R volume (cc)	L/R max Z(x, y, z)
Middle and inferior frontal gyri	9, 46, 6, 44, 45	1.7/0.6	4.9(-37,17,21)/4.5(45,14,16)
Cuneus	23, 18, 30, 17	na/1.5	na/5.2(12, -71,13)
Middle and inferior temporal gyri	21, 37, 19, 39, 22	2.8/2.5	4.9(-56, -24, -18)/5.7(56, -28, -14)
Precentral gyrus	6, 9	0.4/0.2	4.2(-33, -6,50)/3.3(34,9,34)
Superior temporal gyrus	22, 42, 38, 39	0.6/0.4	4.2(-40, -51,19)/3.9(55, -34,11)
Lentiform nucleus		1.3/0.6	3.8(-30, -10, -2)/4.1(22,5,5)
Lingual gyrus and fusiform gyrus	17, 19, 18, 20	1.3/0.6	4.1(-36, -64, -3)/4.0(46, -3, -25)
Precuneus	7	na/0.4	na/3.6(12, -66,41)
Joint source 2, white matter	Brodmann area	L/R volume (cc)	L/R max Z(x, y, z)
Precuneus	7, 31	0.2/1.9	3.2(-24, -50,44)/6.1(25, -53,39)
Middle frontal gyrus	6, 9, 10	3.5/1.3	5.0(-30,7,47)/4.1(28,4,50)
Precentral gyrus	4, 6	0.4/2.4	3.2(-30, -10,61)/4.5(28, -28,61)
Cuneus	18	na/0.9	na/4.5(22, -76,23)
Posterior cingulate	29	0.9/0.2	4.4(-1, -42,12)/3.5(3, -44,15)
Clastrum		0.4/0.9	3.5(-30,11, -8)/4.3(31,7, -8)
Superior and inferior parietal lobules	7, 40	0.6/1.1	4.1(-28, -50,40)/4.1(25, -59,39)
Postcentral gyrus	3	na/0.6	na/3.9(22, -27,62)
Medial and superior frontal gyri	10, 25, 6, 8	2.2/2.4	3.9(-12,64, -3)/3.9(13,61, -4)
Inferior frontal gyrus	47, 46	0.9/0.2	3.7(-15,17, -15)/3.0(25,17, -15)
Fusiform gyrus	20	0.4/0.4	3.4(-49, -23, -25)/3.5(48, -30, -21)
Anterior cingulate and cingulate gyrus	24, 32	0.4/0.2	3.2(-1,25, -4)/.1(24,11,42)
Joint source 3, gray matter	Brodmann area	L/R volume (cc)	L/R max Z(x, y, z)
Supramarginal gyrus	40	1.1/na	8.4(-37, -42,37)/na
Inferior parietal lobule	40	3.2/0.9	7.3(-43, -43,38)/4.7(48, -35,27)
Middle temporal gyrus	37, 39, 19	0.6/2.4	4.3(-31, -67,25)/6.9(40, -57,0)
Medial and middle frontal gyrus	6, 11, 9	3.9/2.2	6.5(-9, -26,69)/4.9(22, -8,47)
Postcentral gyrus	3, 40, 5	2.2/0.2	6.2(-9, -31,69)/3.4(13, -34,68)
Parahippocampal gyrus	Hippocampus, 19, 28, Amygdala, 35, 37, 36, 27	5.2/4.3	6.1(-25, -14, -11)/5.3(40, -51, -2)
Precentral gyrus	6, 9, 4	3.2/0.2	5.7(-13, -21,69)/5.5(36,12,31)
Cuneus, fusiform gyrus and lingual gyrus	18, 37, 19, 17	1.3/3.9	3.7(-25, -88, -17)/5.3(21, -90, -16)
Inferior frontal gyri	9	na/0.4	na/4.4(33,9,27)
Paracentral lobule	6, 31, 4, 5	2.2/1.1	4.8(-3, -33,69)/4.6(3, -29,69)
Lentiform nucleus		1.3/1.5	4.4(-30, -11, -8)/4.8(28, -16, -8)
Uncus	28, 20, 36	0.6/0.2	4.7(-28, -7, -26)/3.3(15, -2, -30)
Insula	13	na/0.6	na/4.5(45, -32,22)

Joint source 1, gray matter	Brodmann area	L/R volume (cc)	L/R max Z(x, y, z)
Orbital gyrus	11	na/0.4	na/3.9(12,43, -20)
Middle, inferior and superior occipital gyri	19, 37, 18	1.0/1.1	4.2(-30, -73,23)/3.9(39, -63,2)
Cingulate gyrus, anterior and posterior cingulate	32, 31, 24	2.1/0.8	3.9(0,33, -10)/3.6(12, -21,45)
Superior and inferior temporal gyri	22, 42, 38, 19	0.4/0.6	3.5(-42, -55,15)/3.7(58, -42,13)
Thalamus		0.9/na	3.5(-13, -23,9)/na
Superior frontal gyrus	9	0.4/na	3.4(-33,45,30)/na
Joint source 3, white matter	Brodmann area	L/R volume (cc)	L/R max Z(x, y, z)
Superior and middle temporal gyri	39, 13, 22, 41, 21, 42, 38, 20, 37	16.0/14.9	18.8(-46, -44,23)/19.4(43, -50,25)
Supramarginal gyrus	40	2.8/2.6	15.6(-48, -48,27)/12.5(49, -48,26)
Inferior parietal lobule	40, 39	3.2/1.9	14.0(-52, -45,23)/5.5(46, -54,36)
Insula	13	2.2/1.9	12.5(-40, -43,21)/9.6(36, -46,19)
Middle frontal gyrus	6, 10, 8, 46, 9, 11, 47	10.6/8.9	11.3(-31,7,45)/8.7(33,8,47)
Superior parietal lobule	7	2.2/na	10.6(-27, -53,41)/na
Fusiform gyrus	20, 37	3.2/2.2	9.4(-42, -14, -23)/7.1(42, -13, -26)
Inferior temporal gyrus	20, 21	3.0/4.1	8.4(-42, -10, -27)/5.8(39, -10, -30)
Middle, inferior and superior occipital gyri	19, 18, 37	2.4/6.6	5.0(-34, -78,5)/8.0(40, -76,3)
Precuneus	7, 31, 19	3.9/5.6	7.4(-22, -50,44)/5.3(13, -69,23)
Superior and medial frontal gyri	6, 8, 11, 10, 9	3.7/1.5	5.2(-15,55, -13)/7.1(33,13,50)
Postcentral gyrus	2, 43, 3, 40, 1	5.6/4.1	6.9(-48, -29,41)/6.5(43, -29,36)
cuneus	18, 7, 23, 17	0.6/3.5	3.3(-25, -92,0)/6.2(13, -68,17)
Precentral gyrus	6, 4, 9, 43	4.1/1.9	5.7(-56,0,21)/4.2(56, -7,13)
Inferior frontal gyrus	46, 47, 9, 44	1.7/1.9	5.6(-33,33,16)/4.8(39,37,9)
Angular gyrus	39	0.6/0.4	3.7(-34, -59,35)/4.5(42, -62,32)
Uncus	20	0.2/0.2	4.5(-37, -13, -31)/3.9(37, -16, -29)
Cingulate gyrus and posterior cingulate	32, 31, 29	2.8/1.9	5.4(-4, -41,16)/5.2(16, -62,17)
Transverse temporal gyrus	42	0.2/0.2	4.3(-61, -11,14)/3.4(56, -13,12)
Joint source 4, gray matter	Brodmann area	L/R volume (cc)	L/R max Z(x, y, z)
Inferior parietal lobule	40	3.0/1.7	8.4(-34, -31,40)/4.2(40, -39,38)
Middle, medial and superior frontal gyri	8, 6, 9, 10, 47, 25, 11	5.1/13.8	4.4(-24,27,37)/7.3(31,14,39)
Postcentral gyrus	3, 2, 40	3.0/1.5	7.1(-30, -34,43)/4.3(48, -30,50)
Inferior frontal gyrus	47, 44, 45, 9	0.6/2.8	3.7(-45,14,16)/5.8(30,29,1)
Superior parietal lobule and precuneus	7	2.2/1.8	5.0(-24, -59,46)/4.4(19, -61,42)
Cingulate gyrus	31, 23, 24, 32	1.5/1.1	4.8(-25, -31,40)/3.6(3, -21,26)
Insula	13	na/0.9	na/4.8(28,25,6)

Joint source 1, gray matter	Brodmann area	L/R volume (cc)	L/R max Z(x, y, z)
Precentral gyrus	9	0.2/0.2	3.6(-33,12,35)/4.6(37,12,39)
Inferior and middle temporal gyri	39, 21, 37, 20, 19	na/3.0	na/5.5(50, -53, -4)
Posterior cingulate	23, 29	0.9/0.6	4.4(-1, -32,24)/3.4(4, -31,24)
Subcallosal gyrus	25	0.2/0.4	3.6(-3,12, -13)/4.3(3,12, -14)
Lingual gyrus	18	0.6/na	3.7(-3, -84, -11)/na
Superior temporal gyrus and angular gyrus	39, 22, 13	na/1.7	na/3.7(31, -53,27)
Fusiform gyrus	36, 37	0.2/0.2	3.7(-49, -40, -23)/3.4(58, -52, -16)
Joint source 4, white matter	Brodmann area	L/R volume (cc)	L/R max Z(x, y, z)
Thalamus		15.1/14.2	20.1(-12, -14,10)/19.1(10, -14,10)
Cuneus	18, 17, 30, 23, 7, 19	8.2/7.3	10.6(-10, -76,15)/7.7(6, -79,16)
Lingual gyrus	18, 17, 19	6.9/1.5	7.9(-16, -80, -2)/4.7(18, -83, -5)
Inferior parietal lobule	40	2.2/0.6	7.1(-31, -47,44)/4.6(31, -37,50)
Caudate		1.5/0.4	7.1(-12, -6,17)/4.9(15, -11,18)
Posterior cingulate	31, 30	2.2/na	6.9(-10, -65,16)/na(0,0,0)
Middle, medial and superior frontal gyri	6, 9, 11, 32, 8	1.9/6.2	4.8(-10, -13,63)/6.5(24,5,47)
Precuneus	31, 7, 19	7.1/2.2	6.5(-9, -69,21)/5.7(22, -76,26)
Superior temporal gyrus	39, 22, 38, 42	2.8/0.2	6.4(-49, -53,22)/3.2(53, -49,11)
Inferior, superior and middle occipital gyri	18, 19	4.7/1.7	6.0(-33, -79, -4)/4.9(31, -85, -6)
Superior parietal lobule	7	0.4/na	5.8(-31, -49,49)/na
Fusiform gyrus	20, 19	1.5/1.7	5.6(-56, -20, -22)/5.4(43, -26, -18)
Inferior frontal gyrus	9, 47	0.2/0.6	3.6(-40,27, -8)/5.4(34,10,27)
Cingulate gyrus	24, 31	0.2/0.4	3.3(-10, -39,41)/5.2(19,8,44)
Parahippocampal gyrus	30, 36, 27, Amygdala, 35	1.1/0.9	5.0(-16, -31, -4)/4.3(39, -29, -20)
Paracentral lobule and precentral gyrus	6, 5, 4	4.6/2.6	5.4(-39, -11,41)/5.2(37,4,27)
Inferior temporal gyrus	20, 37	1.3/1.1	4.7(-59, -24, -19)/4.1(43, -63, -4)
Lentiform nucleus		0.9/0.6	4.7(-21, -11,9)/3.4(31, -14,6)
Middle temporal gyrus	22, 21, 39, 37	1.9/1.3	4.3(-56, -38, -1)/4.7(49, -41,3)
Supramarginal gyrus	40	0.6/na	4.6(-55, -51,22)/na
Postcentral gyrus	3, 4	1.1/0.9	3.6(-24, -29,57)/3.5(34, -34,46)
Rectal gyrus	11	na/0.4	na/3.5(7,35, -22)

Voxels above a threshold of  $|Z| > 3.0$  were converted from Montreal Neurological Institute (MNI) coordinates to Talairach coordinates and entered into a database to assign anatomic labels for the left (L) and right (R) hemispheres. The concentration of voxels in each area is provided in cubic centimeters (cc). Within each area, the maximum Z value and its coordinate are provided.

**Table 2**

White matter determined by the ICBM DTI-81 Atlas

Joint source 1, white matter	Volume (cc)	Percentage	Max Z(x, y, z)
Splenium of corpus callosum	1.06	8.26%	6.36(0, -41,20)
Middle cerebellar peduncle	0.47	2.97%	3.80(17, -24, -30)
Cingulum (cingulate gyrus) right	0.02	1.02%	3.75(8, -45,15)
Cingulum (hippocampus) left	0.10	1.87%	3.64(-16, -37, -3)
Cingulum (hippocampus) right	0.02	1.02%	3.60(8, -45,14)
Anterior limb of internal capsule right	0.04	1.94%	3.32(-13, -28, -13)
Joint source 2, white matter	Volume (cc)	Percentage	Max Z(x, y, z)
Inferior fronto-occipital fasciculus right	0.47	24.65%	4.31(32,7, -9)
Uncinate fasciculus right	0.17	43.36%	4.09(33,2, -10)
Cerebral peduncle right	0.04	3.89%	3.61(-7, -49, -30)
Inferior fronto-occipital fasciculus left	0.15	8.01%	3.49(-30,12, -9)
Superior cerebellar peduncle right	0.06	5.94%	3.42(-7, -43, -31)
Superior cerebellar peduncle left	0.01	1.07%	3.35(8, -49, -30)
Inferior cerebellar peduncle right	0.02	0.34%	3.06(-6, -40, -30)
Splenium of corpus callosum	0.01	0.05%	3.06(-1,41,14)
Joint source 3, white matter	Volume (cc)	Percentage	Max Z(x, y, z)
Superior longitudinal fasciculus right	1.33	19.94%	15.49(38, -52,23)
Superior longitudinal fasciculus left	1.07	16.32%	12.53(-40, -45,23)
Posterior thalamic radiation (include optic radiation) right	0.86	21.43%	10.86(35, -52,23)
Posterior corona radiata right	0.12	3.29%	8.13(33, -52,24)
Splenium of corpus callosum	0.61	4.80%	5.16(-22, -63,17)
Posterior thalamic radiation (include optic radiation) left	0.16	3.84%	5.01(-40, -41,8)
Tapatum right	0.05	8.62%	5.01(32, -48,20)
Cingulum (hippocampus) left	0.15	12.65%	4.63(-10, -45,9)
Retrolenticular part of internal capsule left	0.01	0.41%	3.8(-40, -37,6)
Cingulum (hippocampus) right	0.01	0.80%	3.34(8, -45,12)
Cingulum (cingulate gyrus) right	0.02	0.87%	3.27(8, -45,16)
Uncinate fasciculus left	0.01	1.82%	3.19(-34,2, -19)
Joint source 4, white matter	Volume (cc)	Percentage	Max Z(x, y, z)
Retrolenticular part of internal capsule right	1.87	48.51%	11.67(-18, -15,11)
Posterior limb of internal capsule left	1.80	47.00%	11.19(17, -15,9)
Anterior limb of internal capsule right	0.62	27.46%	8.59(-15, -22, -1)
Cerebral peduncle left	0.55	23.89%	7.49(14, -22, -1)
Fornix (column and body of fornix)	0.17	27.47%	4.97(-1, -7,14)

Joint source 1, white matter	Volume (cc)	Percentage	Max Z(x, y, z)
Superior longitudinal fasciculus right	0.21	3.15%	4.73(33,6,29)
Fornix (cres)/Stria terminalis left	0.10	9.34%	4.65(-21, -31,12)
Cingulum (hippocampus) left	0.10	8.53%	4.41(-18, -34, -3)
Retrolenticular part of internal capsule left	0.05	2.04%	4.34(-24, -25,10)
Superior cerebellar peduncle left	0.09	9.96%	4.26(5, -32, -12)
Superior longitudinal fasciculus left	0.15	2.32%	4.26(-37, -15,38)
Cerebral peduncle right	0.07	7.77%	4.18(-6, -33, -12)
Corticospinal tract right	0.08	3.33%	4.18(23, -22,10)
Splenium of corpus callosum	0.07	0.53%	4.18(-15, -34,12)
Fornix (cres)/Stria terminalis right	0.06	5.73%	4.1(20, -30,12)
Corticospinal tract left	0.19	14.36%	4.1(2, -25, -37)
Middle cerebellar peduncle	0.14	0.88%	4.02(0, -22, -37)
Uncinate fasciculus left	0.21	57.27%	3.86(-35, -1, -18)
Uncinate fasciculus right	0.10	27.43%	3.78(33, -1, -15)
Medial lemniscus right	0.04	3.23%	3.55(-3, -27, -37)
External capsule right	0.18	5.16%	3.39(32, -14,5)
Pontine crossing tract (a part of MCP)	0.03	2.30%	3.39(0, -31, -35)
Cingulum (hippocampus) right	0.01	1.07%	3.23(20, -30, -6)

Voxels above a threshold of  $|Z| > 3.0$  were converted from Montreal Neurological Institute (MNI) coordinates to ICBM DTI81 coordinates and entered into a database to assign anatomic labels. The volume of significant white matter voxels within each fiber tract area is provided in cubic centimeters (cc). The percentage of the fiber tract containing significant white matter voxels is also provided. Within each fiber tract, the maximum Z value and its coordinate are provided.